

# Experimental assessment of effectively probed volume in confocal XRF spectrometry using microparticles

Patricia Poths<sup>1</sup> | Ernesto Chinea-Cano<sup>2</sup> | Naida Dzigan<sup>2</sup> | Iain Gerard Darby<sup>3</sup>  | Janos Osan<sup>3</sup> | Roman Padilla-Alvarez<sup>3</sup> 

<sup>1</sup>University of California, Los Angeles, USA

<sup>2</sup>Environmental Sample Laboratory, International Atomic Energy Agency (IAEA) Laboratories, Seibersdorf, Austria

<sup>3</sup>Nuclear Science and Instrumentation Laboratory (NSIL), International Atomic Energy Agency (IAEA) Laboratories, Seibersdorf, Austria

## Correspondence

Padilla-Alvarez, Roman, Nuclear Science and Instrumentation Laboratory (NSIL), International Atomic Energy Agency (IAEA) Laboratories, Seibersdorf A-2444, Austria.

Email: rpa2000up@hotmail.com

## Present Address

Patricia Poths, University of California, Los Angeles, USA.

Janos Osan, Hungarian Academy of Sciences Centre for Energy Research, Budapest, Hungary.

Current approaches for assessing a confocal micro-X-ray fluorescence-probing volume involve the use of sharp knife edges, thin films, or wires, which are moved through this volume. The fluorescence radiation excited in the material of the object is measured, and profiles are built to enable the determination of the full width at half maximum in any of the three axes of the excited volume. Such approaches do not provide information on the shape of the volume, and the consequent alignment of both used lenses is made based on the position of the maxima of the registered intensity measurements. The use of particles that are smaller than the interaction volume (isolated enough to prevent the influence of nearby particles) and translated through the interaction volume (3D scan) is presented as an alternative methodology to determine the confocal probing volume. Spherical shaped uranium particles with diameter of 1–3  $\mu\text{m}$  originally produced for scanning electron microscopy analysis calibration purposes were used in this study. The results obtained showed that the effectively probed confocal volume has a distinct prolate spheroidal shape that is longer in the axis of the confocal detector than it is wide on the axes of the plane perpendicular to it. The diameter in the longest axis (tilted accordingly to the angle between the two silicon drift detectors) was found to be approximately 25  $\mu\text{m}$ , whereas the shorter was found about 15  $\mu\text{m}$  each, with a volume of about 3,000  $\mu\text{m}^3$ .

## 1 | INTRODUCTION

Capillary optics for focusing X-rays and related systems were developed in early 1990s by Khumakov<sup>[1]</sup> and paved the road for attaining spatially resolved X-ray analysis.<sup>[2,3]</sup> Monolithic X-ray lens consisting of thousands of capillaries, elliptically shaped and bound in to a single piece, served as a focusing element to capture divergent X-rays and

concentrate them at focal spots within a few tens of micrometers. For its introduction into X-ray analytical practice, the initial experimental needs were to assess the transmission efficiency, the gain of lens power density, the uniformity of illumination, angular divergence, and the focal spot size (size of the excitation volume at the sample surface).<sup>[4]</sup>

Different experimental approaches have been followed to assess the focal spot size. For example, an

This is an open access article under the terms of the Creative Commons Attribution License, which permits use, distribution and reproduction in any medium, provided the original work is properly cited.

© 2019 International Atomic Energy Agency. X-Ray Spectrometry published by John Wiley & Sons Ltd.

image of the illuminated spot was obtained in a photographic film or using an X-ray intensifier coupled with a CCD camera and a video capture card.<sup>[4–6]</sup> Scanning a thin metal wire<sup>[4,7–9]</sup> or a sharp edge knife<sup>[10]</sup> through the horizontal and vertical axes and measuring the fluorescence excited in the material allow producing intensity profiles that can be fitted (to establish the width at half of the maximum intensity of the Gaussian shaped curve or the position of the zero value of the differentiated dependence, respectively). Such procedures have become conventional to report the dimensions of the spot size in two axes. The shape of the focal spot is described as a spherical or ellipsoidal, the latter being when the sample is tilted with respect to the lens central axis.

More elaborate procedures for lateral and spectral characterization of the microbeam based on scanning with a small pinhole through the focal plane of its focus or using an ultrahigh-resolution X-ray camera are described in Bjeoumikhov et al. and Kanngießner et al.,<sup>[11,12]</sup> respectively.

The use of half elliptical lenses enables the focusing of divergent X-rays from a small focal spot into parallel beam. If such lens is positioned in front of an X-ray detector, with the half lens capture focus matching the exit focus of the elliptical lens used for focusing the primary beam, the effectively probed volume is reduced, thus achieving a better spatial resolution. Since 2003,<sup>[13]</sup> confocal X-ray fluorescence (XRF) spectrometers have been deployed in several laboratories. The assessment of the confocal probing volume size is usually made by following any of the procedures adopted for micro-XRF but incorporating an additional scan in depth with the measurement of a single or multielement thin foils.<sup>[13–16]</sup>

However, these approaches do not provide information on the shape of the volume, and the consequent alignment of both used lenses is made using the maxima of the registered intensity measurements. The shape of the effectively probed volume has been theoretically described as ellipsoidal with flux intensity following a two-dimensional Gaussian bell function<sup>[17]</sup> or as a prolate spheroid, with polar diameter greater than the equatorial one.<sup>[18]</sup> Expressions for the primary fluorescence intensity of various types of 3D micro-XRF experiments were presented in Malzer and Kanngießner,<sup>[17]</sup> as well as analytical expressions for the sensitivity and a calibration procedure based on using thin films.

The use of particles that are smaller than the interaction volume (and distant enough from each other to prevent the influence of nearby particles) is an alternative to the use of wires, sharp edge knives, and thin films. If such particles are translated through the interaction volume (3D scan), the measurement of their fluorescent intensity can serve to corroborate experimentally the shape of the confocal probing volume by rendering in 3D such results and establishing as a boundary of the confocal volume

accounting a value of counts corresponding three times the observed counting at continuum under the peak.

## 2 | EXPERIMENTAL

The proposed procedure is based on the use of particles that are smaller than the interaction volume (isolated enough to prevent the influence of nearby particles) and translated through the interaction volume (3D scan). Spherical shaped uranium particles with diameter of 1–3  $\mu\text{m}$  originally produced as a reference material for microanalysis were used in this study.

The procedure includes several steps: (a) finding and characterizing isolated (or clusters of two to three) particles by scanning electron microscopy and energy dispersive X-ray spectrometry (SEM-EDS); (b) relocation of the sample to the confocal XRF sample stage; (c) 3D scan through a volume box containing the particle on its center and measurement of the fluorescent intensity; and (d) further rendering of measurement results in 3D maps.

### 2.1 | Uranium particles

The uranium particles were produced for internal use in the Quality Control Program of the Environmental Sample Laboratory, Department of Safeguards, International Atomic Energy Agency (IAEA). The particles were produced out of suitable solutions of uranium compounds using a modified vibration aerosol generator.<sup>[19]</sup> This technique allows to produce monodisperse droplets, which after an oxidation step in a heating column are collected onto suitable substrates. These particles were characterized with microanalytical methods to determine their size, shape, internal morphology, and chemical and structural properties to assess their suitability as a reference material for microparticle analytical methods by mass spectrometry.

The equipment produces a fine aerosol, which is dried and calcined to form particles of uranium with a narrow and reproducible size distribution, density, and shape. For this study, natural uranium particles were selected with an average particle diameter of 1–2  $\mu\text{m}$  and an estimated density of 4  $\text{g}/\text{cm}^3$ . However, the nature of the production process renders agglomerates of varying number of particles. This is particularly attractive for this study because it allows selecting single, double, and triplet particle clusters as needed.

### 2.2 | Scanning electron microscopy and energy dispersive X-ray spectrometry

The SEM used in this work was an XL-30 model (Phillips) using a LaB6 cathode for emission, with secondary and backscatter electron detectors and an EDS. The analysis

of the particles was conducted at 20-kV-accelerating voltage and magnification from 135 to 10,000  $\times$ , with a working distance of 5 mm. Secondary electron images were taken to confirm the shape and location of the particles, and X-ray emission spectra were measured to corroborate the composition of the particles.

The location of each of the particles was recorded in  $x$ - $y$  coordinate units of the SEM sample stage, as well as the coordinates of three reference markers in the sample stage.

### 2.3 | Sample relocation between SEM-EDS and XRF spectrometer

Following the SEM measurements, the samples were transferred to the micro/confocal XRF spectrometer, and the particles of interest were relocated using the three-point algorithm described in Admon.<sup>[20]</sup> The principle in this algorithm assumes that no nonlinear distortion of the sample takes place during the transfer between the two instruments and is usually referred to as the triangulation method. The inaccuracy in coordinates for each of the sample stages was assessed by moving the stage away to a random position and returning 10 times to the desired coordinates. In the SEM images, the displacement of the center of the particle was measured in the secondary electron images, whereas in micro-XRF, the coordinates of the new position were found by performing  $x$ - $y$  scans.

### 2.4 | Micro-XRF and confocal XRF spectrometer

The measurements were performed with a microbeam-scanning XRF/X-ray absorption spectrometer designed and constructed in the IAEA Laboratories, Seibersdorf, Austria.<sup>[21]</sup> The spectrometer has been upgraded by the addition of a silicon drift detector (SDD) and a polycapillary conical lens for confocal XRF measurements. The main features of the instrument and the results of testing different focusing optics devices are described in Wegrzynek et al.<sup>[22]</sup> The spectrometer (see Figure 1) after such modifications consists now of the following:

- (a) an Mo-anode X-ray tube (3 kW and 60 kV) and a monolithic glass polycapillary lens (X-Ray Optical Systems, Inc.) for focusing the primary excitation beam. The position of the lens can be manually adjusted by tuning a holder ( $xy$  translation and  $x_\phi y_\phi$  tilt) that is attached to the X-ray tube exit window.
- (b) two SDDs (10 mm<sup>2</sup>, 450- $\mu$ m thickness, 8- $\mu$ m Be window, energy resolution of 135 eV at 5.9 keV, and shaping constant of 1  $\mu$ s). The first detector (SDD1) not only is used for micro-XRF measurements but also holds on its measurement head a holder with a polycapillary conic collimator (IfG-Institute for

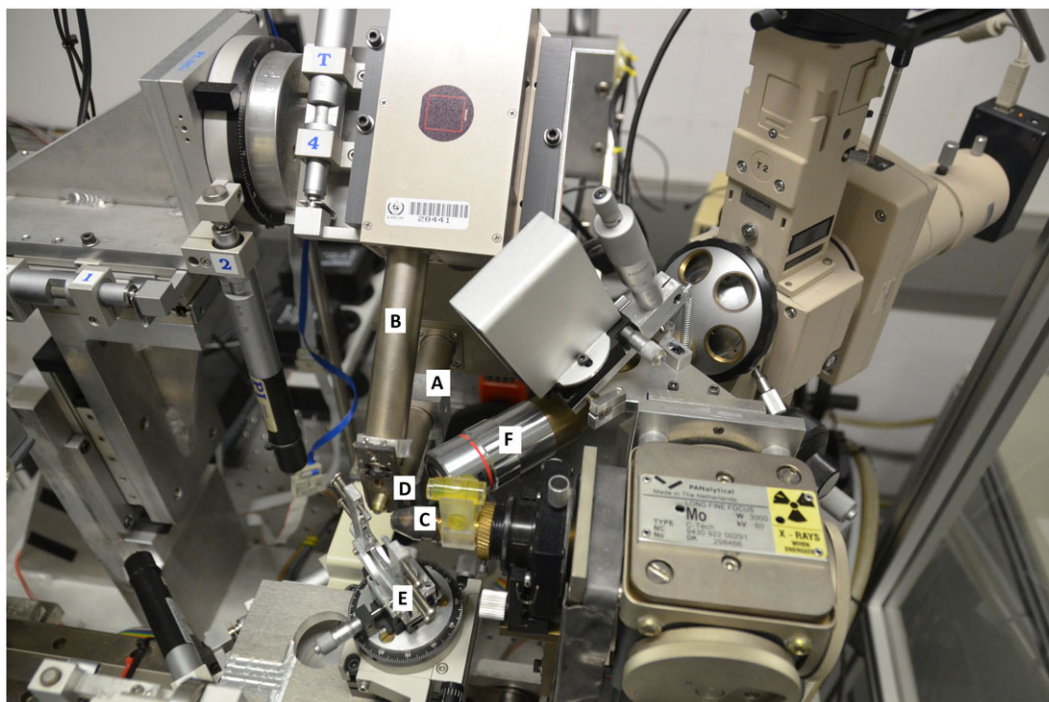


**FIGURE 1** Photograph of the IAEA-NSIL micro/confocal X-ray fluorescence spectrometer. (a) Silicon drift detector used for confocal measurements; (b) silicon drift detector used for micro-X-ray fluorescence measurements; (c) polycapillary lens in the excitation channel; (d) conical lens in front of confocal detector. (e) Motorized sample stage; (f) microscope camera

Scientific Instruments GmbH, Berlin, Germany) aligned as to capture emission from the excited volume toward the second detector (SDD2). SDD1 is mounted in a motorized holder (xyz translation and  $z_\phi$  tilt) that allows the alignment of the conical collimator as to make its focal spot to match with that of the polycapillary lens used for excitation.

- (c) an optical microscope with attached CCD camera, a laser distance sensor.
- (d) a motorized sample stage (xyz translation and  $\theta$  rotation) and a PC-controlled data acquisition system.
- (e) The measurements were performed with the Mo-anode X-ray tube operated at 45 keV and 40 mA. The nominal size of the electron spot on the tube anode is  $12 \times 0.4$  mm. All the measurements were performed in air.

### 3 | RESULTS

#### 3.1 | Finding and characterizing particles

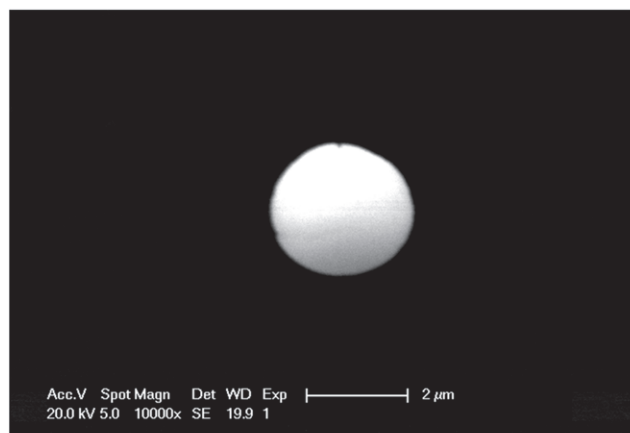
For SEM-EDS analysis, a Mylar film containing the deposited particles was coated with gold. The particles were inspected as to determine their size and composition and to validate their isolation (not closer from each other by less than  $50 \mu\text{m}$ , for example, twice the suspected XRF confocal volume size). The distribution of the particles deposited in the Mylar was found to consist of isolated spheroidal particles with 1- to  $3\text{-}\mu\text{m}$  diameter (example is provided in Figure 2a) or in large or small clusters (see Figure 2b).

The location of the single particles or small clusters (two to three particles) in the microscope stage was recorded for further relocation in the micro-XRF sample stage.

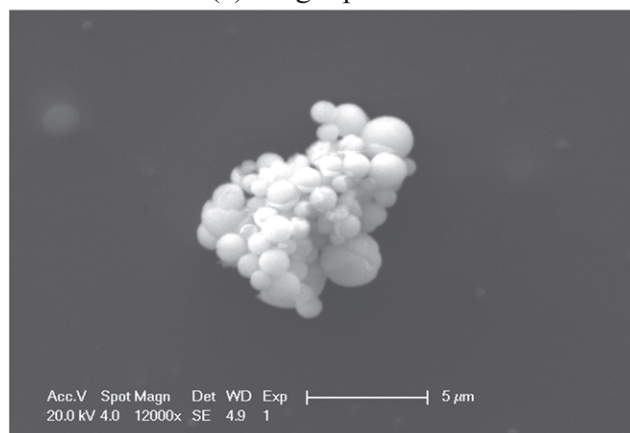
The composition of the particles was found by measuring their X-ray emission using the Energy Dispersive X-Ray Spectrometry (EDXRS). The major constituent is uranium (see Figure 3), and the observed Au peaks are because of the coating of the sample.

#### 3.2 | Relocation of the particles in the XRF sample stage

The sample containing the particles was placed in the micro-XRF sample stage, and the coordinates in the new reference system were calculated using the procedure described by Admon.<sup>[19]</sup> Once the stage was translated as to position the particle in the focal spot, bidimensional area scans ( $x$ - $y$  plane) were made as to define with more accuracy the coordinates of the center of the particle by following the same procedure used in



(a) Single particle



(b) Clustered particles

**FIGURE 2** Examples of secondary electron images of uranium particles

scans of thin wires. An additional scan was made in the  $x$ - $z$  plane to find the center in the axis  $z$ .

The accuracy of the relocation procedure was evaluated by repeating this procedure five times, by moving the stage randomly away from the region by at least  $2.5$  mm. Subsequently, the two-dimensional scans were started returning the stage back to the desired coordinates. The results of such evaluation are presented in Table 1.

The variation in  $x$ -axis and  $z$ -axis was found to be around  $1\text{--}2 \mu\text{m}$ , whereas in  $y$ -axis, the accuracy was  $4\text{--}5 \mu\text{m}$ . The larger variation in  $y$ -axis may be attributed to the fact that the motor for adjusting  $y$  bears all the weight of the sample stage. This accuracy was considered sufficient for defining the boundaries of the volume to be scanned further.

#### 3.2.1 | 3D scan and measurement of the fluorescent intensity

The micro-XRF was calibrated using a tungsten wire cross and a UF4 foil (MicroMatter Technologies Inc.<sup>[23]</sup>)

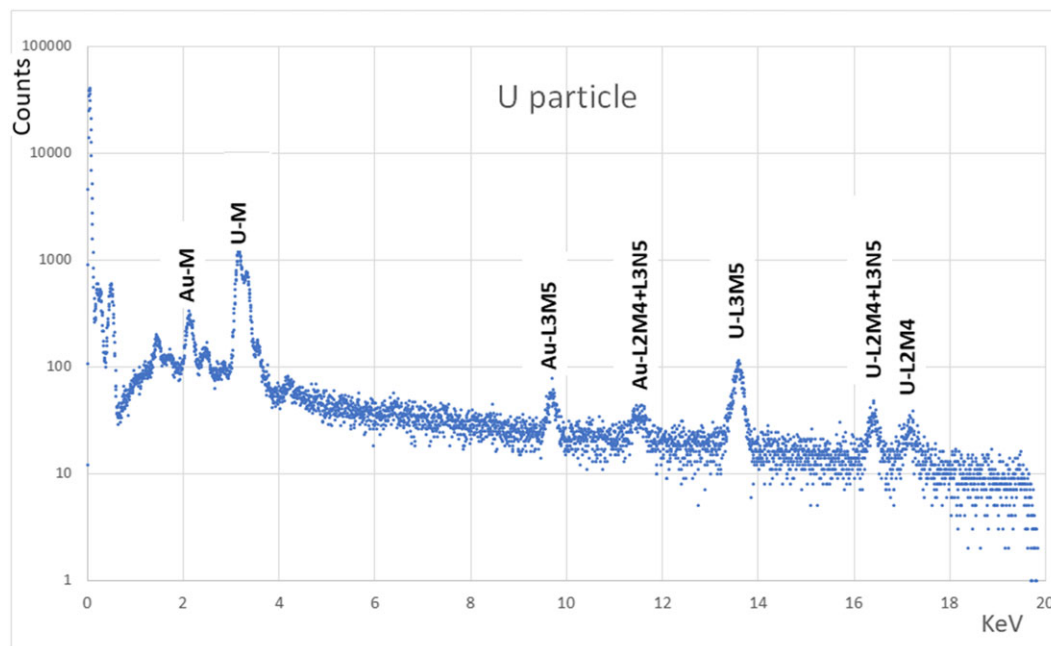


**FIGURE 3** X-ray emission from particles

**TABLE 1** Evaluation of accuracy of micro-X-ray fluorescence positioning

| Coordinates of particle center | <i>x</i> (mm) | <i>y</i> (mm) | <i>z</i> (mm) |
|--------------------------------|---------------|---------------|---------------|
| Average                        | 4.523         | −12.011       | −13.663       |
| Standard deviation             | 0.001         | 0.005         | 0.002         |

to ensure that the location of the excitation beam matched the foci of both lenses as set in the control/measurement software and that the confocal volume was where it was expected to be.

On the basis of the counting statistics observed for the UF4 foil and the certified mass areal density ( $50.7 \mu\text{g}/\text{cm}^2$ ), a preliminary assessment of the instrument sensitivity was made. The mass of individual particles was very small for the confocal XRF absolute detection limits and required long measurement times. Therefore, it was decided to use clusters of two to three particles, having a total volume still small enough so to be smaller than the expected confocal probing size.

The volume scanned for each cluster of particles was set to  $100 \times 76 \times 40 \mu\text{m}$  in volume, with a step size of  $2 \mu\text{m}$  for translation in all the directions, giving data for  $50 \times 38 \times 30$  voxels, and with a measurement time of 5 s. The size in the *x*-axis is larger because of the tilt of the sample under  $45^\circ$  regarding the excitation lens central axis. Before the 3D scans are performed, the coordinate boundaries for the box volume to be scanned were

established as to position the cluster of particles as close to its center as possible.

The counts in two regions of interest were calculated in both the micro-XRF and confocal XRF-collected spectra, corresponding to the energies of Au-L $\alpha$  and U-L $\alpha$ . The data results were exported to an Amira files (.am) containing coordinates and the Region Of Interest (ROI) counts. These files were imported to the Avizo 7.0 software for 3D visualization of the results. The obtained 3D-rendered images are illustrated in Figure 4. The boundaries of the depicted volumes were set at six counts, twice the critical level corresponding to having only 5% probability of measuring nonzero counts in the absence of a true signal (assuming a Poisson probability distribution for the ROI counts in the measured spectra). This procedure differs from the convention of using counts at half of maximum of the thin-film scans and provides a better profile of the volume comprising all the effectively excited and measured volume.

Figure 4a corresponds to the measurement performed with the detector used in micro-XRF mode. It clearly depicts the shape of the excitation beam as a cylinder (corresponding to the measured U-L $\alpha$  counts) with very small variation in diameter. The size of the excitation beam in *x*-*y* plane corresponds to that obtained with the procedure based on scanning a thin wire:  $37 \times 25 \mu\text{m}$ , as reported previously in Wegrzynek et al.<sup>[22]</sup> The layer parallel to plane *x*-*y* in Figure 4a corresponds to the signal arising from the gold coating of the Mylar film detected with the confocal detector. Figure 4b depicts the location of the confocal effectively probed volume.

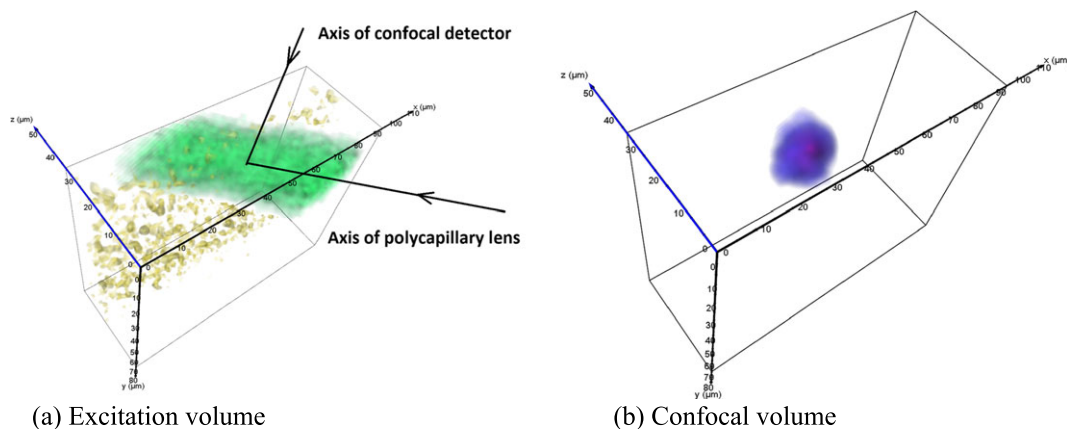


**FIGURE 4** 3D rendering of measured intensities with (a) micro-X-ray fluorescence detector and (b) confocal detector. Volumes represent in Figure 4a (green: U-L $\alpha$  arising from the particles when traversing the excitation volume; yellow: Au-L $\alpha$  from the coating layer when traversing the excitation volume) and in Figure 4b (U-L $\alpha$  arising from the particles when traversing the confocal volume)

The effectively probed confocal volume has a distinct prolate spheroidal shape as described by Cordes et al.<sup>[18]</sup> that is longer in the axis of the confocal detector than it is wide on the axes of the plane perpendicular to it. It is oriented at angles to each axis, and the projections in the  $x$ ,  $y$ , and  $z$  would be distorted giving the impression of a larger volume.

The confocal probing volume for three different particle clusters was found quite similar, showing that there was good reproducibility in the procedure. The diameter in the longest axis (tilted accordingly to the angle between the two SDDs) was found to be approximately 25  $\mu\text{m}$ , whereas the shorter (see Figure 5) was found about 15  $\mu\text{m}$  each, with a volume of about 3,000  $\mu\text{m}^3$

(calculated using a relevant functionality of the Avizo software). The irregularities found in the shape of the volume are conditioned by the low-counting statistics and by the irregular shape of the particles cluster.

The advantages of using this procedure to assess the confocal volume are several. First, it allows one to define the resolution of the confocal analysis with better accuracy, as compared with the use of either wire or thin-film measurement-based methods, for which the standard procedure is reporting the width at half maximum intensity in each of the axes. Table 2 summarizes the results reported for each of these procedures and incorporates in the last row the results from this work for comparison.

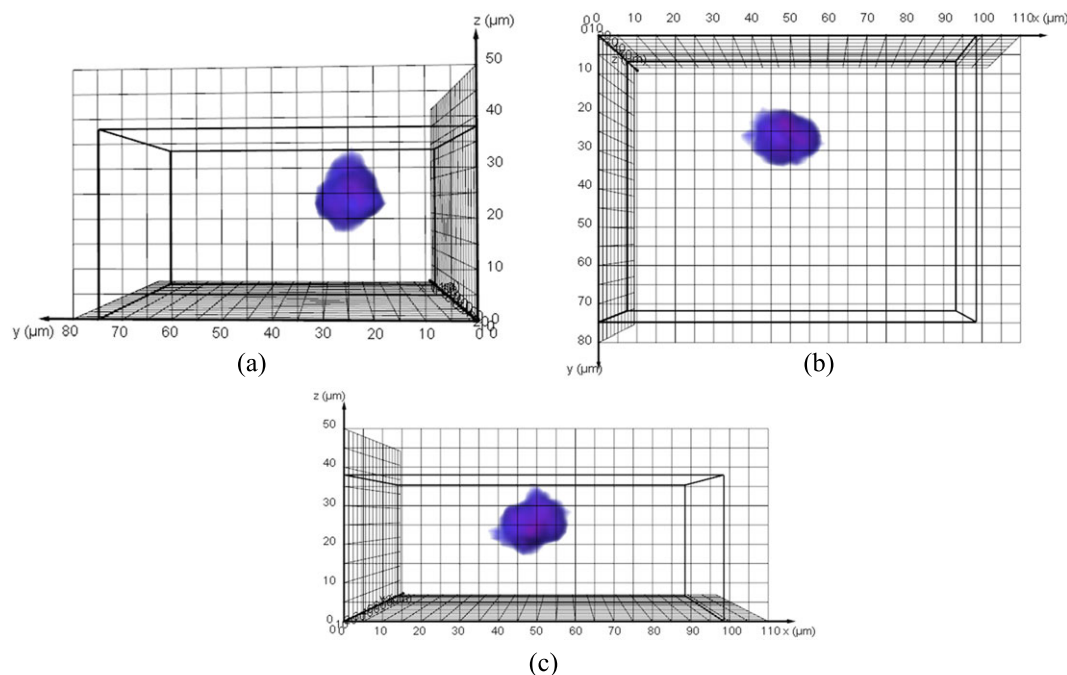


**FIGURE 5** 3D-rendering projections in planes (a)  $y$ - $z$ ; (b)  $x$ - $z$ ; and (c)  $x$ - $y$

**TABLE 2** Comparison of results obtained by conventional procedures used to estimate the confocal volume

| Reference                             | X-ray source                           | Focusing element             |                          | Object used for measurement              | Step size used for scan ( $\mu\text{m}$ ) | Confocal volume dimensions (at energy) <sup>a</sup> |                     |                     |                                    |
|---------------------------------------|--|------------------------------|--------------------------|--|---|---|---------------------|---------------------|------------------------------------|
|                                       |  | Excitation channel           | Detection channel        |  |   | x ( $\mu\text{m}$ )                                 | y ( $\mu\text{m}$ ) | z ( $\mu\text{m}$ ) | Probing volume ( $\mu\text{m}^3$ ) |
| Kanngießer et al. <sup>[13]</sup>     | 7-T wavelength shifter beamline        | PCH                          | PCCC                     | 2- $\mu\text{m}$ Cu foil                 | 5   | 55  | 35                  | n.r.                | n.r.                               |
|                                       | BAMline, BESSY II                      | 30 $\mu\text{m}$<br>17.4 keV | 20 $\mu\text{m}$         |  |   | (8.04 keV)  |                     |                     |                                    |
| Vekemans et al. <sup>[14]</sup>       | ID18F, ESRF                            | CRL                          | PCH                      | 0.5- $\mu\text{m}$ thin glass            | 5   | 7   | 3                   | 20 (Ca-Ka)          | n.r.                               |
| Laszlo et al. <sup>[15]</sup>         | 1-2 $\mu\text{m}$ (y)                  | 3-10 $\mu\text{m}$ (x)       | 20 $\mu\text{m}$         | NIST SRM 1832                            |   | (28 keV)  |                     | 10 (Sr Ka)          |                                    |
|                                       |  |                              |                          |  |   |   |                     | 35 (Ca-Ka)          | 150-350                            |
| Patterson et al. <sup>[16]</sup>      | X-ray tube, Ag anode<br>50 kV, 0.5 mA  | PC                           | PC                       | 10- $\mu\text{m}$ Ta foil                | n.r.                                      | 30  | 30                  | 65                  | n.r.                               |
| Malzer and Kanngießer <sup>[17]</sup> | n.r.                                   | PCC<br>15 $\mu\text{m}$      | PCCC<br>20 $\mu\text{m}$ | Theoretical calculation                  | 5   |   |                     | 25 <sup>(b)</sup>   | n.r.                               |
| Cordes et al. <sup>[18]</sup>         | X-ray tube, Ag anode<br>45 kV, 0.45 mA | PC                           | PC                       | Theoretical description                  | n.r.                                      | 30  | 30                  | 55                  | n.r.                               |
| This work                             | X-ray tube, Mo anode<br>45 kV, 40 mA   | PC                           | PCCC<br>25 $\mu\text{m}$ | 1- to 3- $\mu\text{m}$ uranium particles | 2   | 25  | 15                  | 15                  | 3,000                              |
|                                       |  |                              |                          |  |   | (13.6 keV)  |                     |                     |                                    |

Note. CRL: compound refractive lenses; n.r.: not reported; PC: polycapillary monolithic lens; PCCC: polycapillary conical collimator; PCH: polycapillary half lens.

<sup>a</sup>In all cases, excitation beam impinges the sample surface under 45°; detector axis is perpendicular to excitation.

<sup>b</sup>Calculated based on assumption of ellipsoidal shape for the confocal volume.

Additionally, in the used experimental setup, where the confocal detector is tilted in respect to the horizontal plane, it allows one to define the exact tilt of the confocal volume.

The use of such procedure could also serve to measure the intensity of excitation radiation within the confocal volume to validate the prediction using the formulae described in Malzer and Kanngießer.<sup>[17]</sup>

## 4 | CONCLUSIONS

The proposed procedure to assess the shape and dimensions of effectively probed volume in confocal XRF by measuring microparticles complements the conventional procedures of scanning wires or thin films. When the particles are translated through the interaction volume (3D scan), the measurement of their fluorescent intensity serves to determine the confocal probing volume by further rendering in 3D the counting results.

An experimental definition of the shape, orientation, and dimensions of the probing volume was obtained, resulting in a prolate spheroidal shape. The dimensions of the confocal probed volume were found approximately 25- $\mu\text{m}$  diameter in the longest axis (e.g., that tilted accordingly to the angle between the two SDDs) and of 15- $\mu\text{m}$  diameter in each of the other perpendicular axes. The resulting probing volume was estimated to be about 3,000  $\mu\text{m}^3$ .

## ACKNOWLEDGEMENTS

The experimental work was conducted as part of an internship program at Nuclear Science and Instrumentation Laboratory, Department of Nuclear Sciences and Applications, International Atomic Energy Agency. Ms Poths deeply thanks the NSIL for the provided opportunity.

## ORCID

Iain Gerard Darby  <https://orcid.org/0000-0003-2091-2616>  
Roman Padilla-Alvarez  <https://orcid.org/0000-0002-6835-9875>

## REFERENCES

- [1] M. A. Kumakhov, F. F. Komarov, *Phys. Rep.***1990**, 191(5), 289.
- [2] A. Rindby, *X-Ray Spectrom.***1993**, 22, 187.
- [3] K. Janssens, L. Vincze, J. Rubio, F. Adams, G. Bernasconi, *J. Anal. At. Spectrom.***1994**, 9, 151.
- [4] Y. Yan, *Adv. X-Ray Anal.***1996**, 40, 542.
- [5] A. Attaelmanan, A. Rindby, P. Voglis, A. Shermeat, *Nucl. Instr. and Meth. B.***1993**, 82, 481.
- [6] J. Gormley, T. Jach, E. Steel, Q. F. Xiao, *Adv. X-Ray Anal.***1997**, 41, 239.
- [7] B. Vekemans, K. Janssens, G. Vittiglio, F. Adams, L. Andong, Y. Yiming, *Adv. X-Ray Anal.***1997**, 41, 278.
- [8] M. Lankosz, J. Sieber, *Rev. Sci. Instrum.***2000**, 71(7), 2640.
- [9] B. Laforce, B. Vermeulen, J. Garrevoet, B. Vekemans, L. Van Hoorebeke, *Anal. Chem.***2016**, 88, 3386.
- [10] G. Buzanich, P. Wobrauschek, C. Strelti, A. Markowicz, D. Wegrzynek, E. Chinea-Cano, S. Bamford, *Spectrochim. Acta, Part B.***2007**, 62(11), 1252.
- [11] B. Kanngießer, N. Kemf, W. Malzer, *Nucl. Instrum. Methods Phys. Res., Sect. B.***2002**, 198(3–4), 230.
- [12] A. Bjeoumikhov, M. Erko, S. Bjeoumikhova, A. Erko, I. Snigireva, A. Snigirev, T. Wolff, I. Mantouvalou, W. Malzer, B. Kanngießer, *Nucl. Instrum. Methods Phys. Res., Sect. A.***2008**, 587(2–3), 458.
- [13] B. Kanngießer, W. Malzer, I. Reiche, *Nucl. Instrum. Methods Phys. Res., Sect. B.***2003**, 211(2), 259.
- [14] B. Vekemans, L. Vincze, F. E. Brenker, F. Adams, *J. Anal. At. Spectrom.***2004**, 19, 1302.
- [15] V. Laszlo, B. Vekemans, F. E. Brenker, G. Falkenberg, K. Rickers, A. Somogyi, M. Kersten, F. Adams, *Anal. Chem.***2004**, 76, 6786.
- [16] B. M. Patterson, K. A. Defriend Obrey, G. J. Havrilla, A. Nikroo, H. Huang, *Fusion Sci. Technol.***2009**, 55(4), 417.
- [17] W. Malzer, B. Kanngießer, *Spectrochim. Acta Part B.***2005**, 60, 1334.
- [18] N. L. Cordes, G. J. Havrilla, I. O. Usova, K. A. Obrey, B. M. Patterson, *Spectrochim. Acta Part B.***2014**, 101, 320.
- [19] R. Middendorp, M. Dürr, A. Knott, F. Pointurier, D. Ferreira Sanchez, V. Samson, D. Grolimund, *Anal. Chem.***2017**, 89(8), 4721.
- [20] U. Admon, Single Particles Handling and Analyses. In: Oughton D. H., Kashparov V. (eds) *Radioactive Particles in the Environment*. NATO Science for Peace and Security Series C: Environmental Security. Springer, Dordrecht 2009.
- [21] D. Wegrzynek, A. Markowicz, S. Bamford, E. Chinea-Cano, M. Bogovac, *Nucl. Instrum. Methods Phys. Res., Sect. B.***2005**, 231, 176.
- [22] D. Wegrzynek, R. Mroczka, A. Markowicz, E. Chinea-Cano, S. Bamford, *X-Ray Spectrom.***2008**, 37, 635.
- [23] <http://www.micromatter.com/index.aspx>

**How to cite this article:** Poths P, Chinea-Cano E, Dzigal N, Darby IG, Osan J, Padilla-Alvarez R. Experimental assessment of effectively probed volume in confocal XRF spectrometry using microparticles. *X-Ray Spectrometry*. 2019;48: 553–560. <https://doi.org/10.1002/xrs.3045>